Vessel Visualization using Curvicircular Feature Aggregation

G. Mistelbauer[1], A. Morar[2], A. Varchola[1], R. Schernthaner[3], I. Baclija[4], A. Köchl[4], A. Kanitsar[5], S. Bruckner[6], E. Gröller[1]

[1]Vienna University of Technology, Austria
[2]University Politehnica of Bucharest, Romania
[3]Medical University of Vienna, Austria

[4]Kaiser-Franz-Josef Hospital Vienna, Austria
[5]VISUAPPS GmbH
[6]University of Bergen, Norway

Abstract
Radiological investigations are common medical practice for the diagnosis of peripheral vascular diseases. Existing visualization methods such as Curved Planar Reformation (CPR) depict calcifications on vessel walls to determine if blood is still able to flow. While it is possible with conventional CPR methods to examine the whole vessel lumen by rotating around the centerline of a vessel, we propose Curvicircular Feature Aggregation (CFA), which aggregates these rotated images into a single view. By eliminating the need for rotation, vessels can be investigated by inspecting only one image. This method can be used as a guidance and visual analysis tool for treatment planning. We present applications of this technique in the medical domain and give feedback from radiologists.

Categories and Subject Descriptors (according to ACM CCS): I.3.3 [Computer Graphics]: Picture/Image Generation—Display algorithms I.3.7 [Computer Graphics]: Three-Dimensional Graphics and Realism—Raytracing I.4.6 [Image Processing and Computer Vision]: Segmentation—Edge and feature detection

1. Introduction

Radiological investigations often require a fast and precise diagnosis for proper treatment planning in order to minimize negative impacts on a patient's health state. One particular field of radiology is the analysis of blood vessels, for example, the identification of deviations of the flow channel in case of peripheral arterial occlusive diseases. Blood flow deviations can be caused by pathologies on the vessel walls, such as calcifications or soft plaque. Angiographic medical volume data are typically acquired using Computed Tomography Angiography (CTA) or Magnetic Resonance Angiography (MRA). These data consist of stacks of axial sections or slice images. The usual radiological diagnostic procedure is the investigation of every axial slice image of a data set, one by one. This is a time consuming task since a typical data set may consist of thousands of slices.

In order to alleviate clinicians from inspecting data sets slice-by-slice, Maximum Intensity Projection (MIP) has evolved to a well established visualization technique for medical investigations. It projects 3D information onto one static 2D image. Applied to CTA data, the method captures bones and calcifications, because they have the highest intensity. However, one cannot distinguish between vessels being blocked by calcifications or vessels having calcifications only on their walls. To remedy this drawback,

Curved Planar Reformation (CPR) techniques were investigated [KFW*02, KFWG06]. These methods depict a curved cut through the lumen of a vessel along its centerline. By rotating around the centerline, the whole lumen of the vessel can be inspected. However, this approach still requires a substantial degree of interaction, making the analysis of a pathology a time consuming process.

The main idea of Curvicircular Feature Aggregation (CFA) is to reduce the amount of necessary interaction by performing an aggregation around the centerline of a vessel. The result is a single static image making the rotation operation unnecessary. Additionally, we support users with visual analysis tools for further inspection of interesting regions. For example, we show additional linked views, such as an axial slice view. Contextual information outside the vessels can be visualized using common techniques such as MIP, Maximum Intensity Difference Accumulation (MIDA) or Direct Volume Rendering (DVR).

The paper is structured as follows. Section 2 gives an overview of related work. The concept of the proposed technique is detailed in Section 3 and the corresponding visual mapping is described in Section 4. Results are presented in Section 5 and limitations are discussed in Section 6. Domain expert feedback is provided in Section 7 and the paper is concluded in Section 8.

MIP	CFA	CPR
+ 1 image	+ 1 image	− many images
+ context	+ context	− context
− occlusions	+ cut along vessel	+ cut along vessel
− location	− location	+ location

Figure 1: *Unifying aspects of Curvicircular Feature Aggregation (CFA) with respect to MIP and CPR.*

2. Related Work

The technique proposed in this work combines several aspects of MIP and CPR, as outlined in Figure 1. The goal is to provide an overview of the whole vasculature and to support clinicians to identify and report vessel pathologies.

Vessel Visualization. Among techniques for the visualization of vascular structures are volume rendering, surface rendering, and vessel flattening. The most commonly used technique for the diagnosis of vascular diseases is Maximum Intensity Projection (MIP). The interpretation of spatial relations can be hindered by artifacts due to inhomogeneities in the contrast agent distribution and aliasing problems caused by the data resolution [KBF*08]. Model-based surface rendering requires knowledge about the centerline and the radius of the vascular structure. The vessel surface can be approximated by geometric primitives such as generalized cylinders [KPL94] or truncated cones [HPSP01]. For a better approximation, B-splines [HPP*00], convolution surfaces [BS91] or subdivision surfaces [DKT98, FWB04] can be used. Wua et al. [WMM*10] present a surface rendering approach for visualizing vascular structures defined by the centerline and the radius. They propose a bidirectional adaptive sampling strategy to generate a topologically-correct base mesh. Model-free methods make no assumption about the vessel cross-section. They extract an iso-surface based on a threshold. Marching cubes [LC87] is the standard choice for surface construction based on iso-values. Termeer et al. [TOBB*07] describe the volumetric bull's eye plot. It is a visualization technique for investigating coronary artery diseases by providing an overview of healthy and scar tissue together with the coronary arteries. They unfold and reformat the myocardium to a cylinder and project it along its major axis. Borkin et al. [BGP*11] propose a 2D vessel visualization method. They introduce a 2D tree diagram representation that shows all the data in one image, while providing anatomical information such as vessel diameter and branching structure. Further information on vessel visualization and quantification can be found in the surveys by Bühler et al. [BFC04] and by Preim and Oeltze [PO07].

Curved Planar Reformation. Planar cuts through the data set are intended to provide more insight into otherwise obscured internal structures. Kanitsar et al. [KFW*02] investigate Curved Planar Reformation (CPR) as a curved cut through a data set along a given path. They intro-

duce three different types of CPR (projected, stretched, and straightened), which exhibit distinct properties. The projected CPR is neither isometric nor conformal, whereas the stretched CPR is conformal. The straightened CPR is isometric and perspective occlusions due to rotations cannot occur, but the spatial perception of the vasculature as a whole is reduced. The untangled CPR, proposed by Kanitsar et al. [KWFG03], uses spatial deformation to avoid occlusions when projecting the vessel tree. The Multipath Curved Planar Reformation (mpCPR) technique, developed by Kanitsar et al. [KFWG06] and evaluated by Roos et al. [RFK*07] was initially designed to investigate peripheral arterial occlusive diseases in the arteries of the lower extremities. Kanitsar et al. [KFWG06] describe a spiral CPR which shows the interior of the vessel by flattening it along a spiral. This method preserves isometry, but lacks spatial context. Lampe et al. [LCMH09] present a more general curve centric reformation. Their method transforms the space around a curve and accomplishes visualizations that are similar to planar reformations used for virtual endoscopy. Methods for virtual endoscopy often use flattening methods based on non-linear rendering, more specifically curve-centric radial ray casting. These visualizations usually map the volume to 2D reformations. The horizontal axis represents the position along the centerline and the vertical axis represents the angular position of the flattened tubular structure displayed from the perspective of the centerline. Bartrolí et al. [BWKG01] discuss a two-step method for colon flattening. Hong et al. [HGQ*06] propose a method for colon flattening which preserves angles and minimizes global distortion. Williams et al. [WGC*08] present a technique for colon visualization based on a combination of CPR and DVR. Our approach renders the vessels straightened and arranges them horizontally in an anatomically sorted manner.

Non-linear Rendering. Gröller [Grö95] investigates methods for non-linear ray tracing with iterative or hierarchical ray representations and discusses their possible applications for visualization of various dynamic systems. Kurzion and Yagel [KY95] present a space deformation for volume visualization based on ray deflectors. Weiskopf et al. [WSE04] implement non-linear ray tracing on the GPU. Their approach consists of a ray setup according to camera parameters, ray integration, ray-object intersection, and local illumination. Wang et al. [WZMK05] discuss a method for volume visualization with non-linear camera projections. It uses a lens-based deformation in order to magnify an interesting object in the scene. Löffelmann and Gröller [LG96] describe an extended camera concept that is able to create artistic effects with ray tracing while maintaining an overview of the scene. Hsu et al. [HMC11] propose a rendering framework for multi-scale rendering of geometric and volumetric models. Their method can present complex structures with multiple levels of detail using a focus+context approach. They also employ artistic effects that are commonly used by illustrators. Non-linear rendering methods, such as
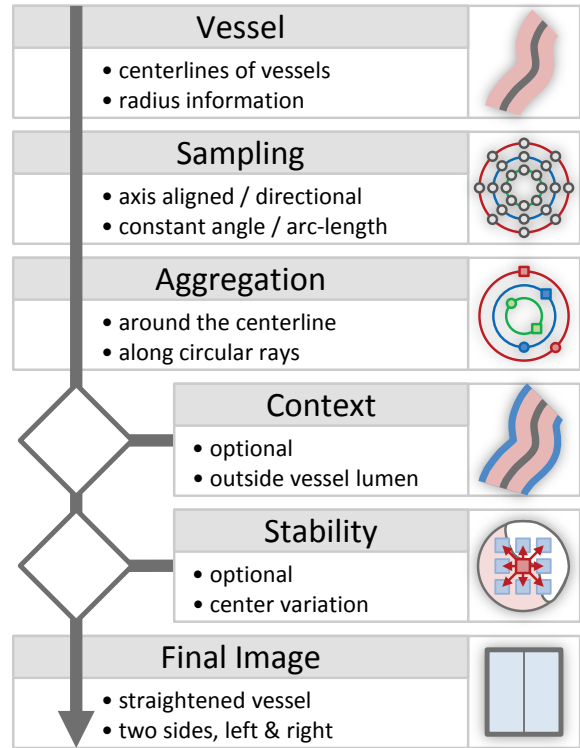
non-linear ray tracing or ray casting, apply concepts of space deformation. In our work we present a technique that also uses non-linear rays for generating images, but it is designed as a diagnostic vascular visualization method.

3. Curvicircular Feature Aggregation

Diagnostic visualization plays an important role in conveying the information in the data to domain experts. The acquired data usually results from an angiographic imaging source, where a contrast agent is used beforehand in order to enhance the vasculature. The imaging source can be, for example, CTA or MRA. Although Digital Subtraction Angiography (DSA), the current gold standard for vascular diagnosis, is a non-tomographic technique, tomographic methods, such as CPR [KFW*02], are gaining in importance. Many CPR images have to be generated from different viewing angles for investigating the lumen of a vessel. Clinicians usually scroll through these images to search for possible pathologies. Motivated by this, we propose Curvicircular Feature Aggregation (CFA) that removes the need to rotate around the vessel centerline. It aggregates rotated views into a single static image. The workflow of CFA is outlined in Figure 2. The vessel centerlines and radii are obtained by radiological assistants in their daily clinical routine. Among many existing vessel tracking techniques, the assistants use a semi-automatic procedure, which is based on the work presented by Kanitsar et al. [KFW*01].

In order to aggregate around the centerline of a vessel, circular rays are cast. These rays are concentric circles with increasing radii, starting from the centerline of the vessel. They can either be axis-aligned or follow the centerline. This is an extension of the CPR technique in order to provide only a single image for several viewing angles. Samples are generated along these circular rays, either at a constant angle or a constant arc-length. As the latter produces more samples on circles with larger radii, it consumes significantly more computing power. Next, the samples are aggregated into one value for every circular ray. This can be achieved by MIP, Minimum Intensity Projection (MINIP) or Average Intensity Projection (AVG). Basically, any common operator can be applied here. MIP and MINIP are of particular clinical relevance, as MIP depicts calcifications while MINIP provides information about soft plaque. Both pathologies are of high importance, since they hinder blood from flowing through a vessel. To provide additional information about how slight variations of the centerline affect the aggregation, our approach also includes a stability visualization, which is combined with the CFA. Finally, the CFA of the lumen can be embedded into a visualization of its anatomical context if radius information is available.

Typical clinical reporting does not only consist of inspecting images generated from CPR or mpCPR, but also requires the consideration of axial images. This has a significant impact on the outcome of a report, as shown by the study of

Figure 2: *Workflow of CFA.*
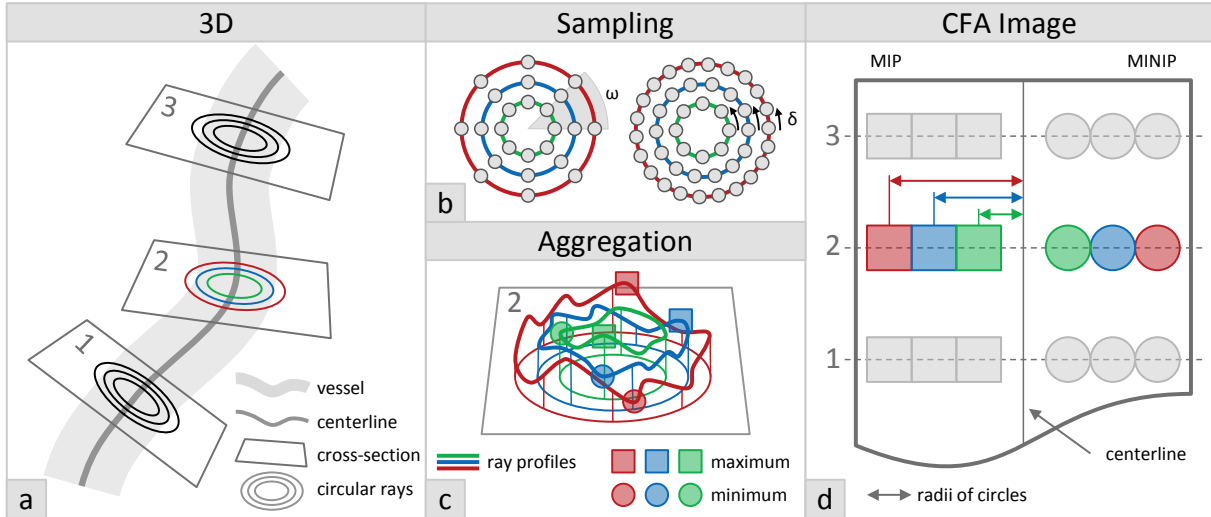
Portugaller et al. [PSH*04]. It is not sufficiently accurate to base a report solely on CPR or MIP images. For this reason, we additionally provide a 3D overview visualization of the vasculature and an axial slice view. By linking these views together with the CFA, users are able to navigate through and explore the vessel tree. In the following sections, each step of Figure 2 will be explained in detail.

3.1. Sampling

To obtain an aggregated value along the circular rays, they are placed in a plane and sampled. We use planar radial sampling due to the cylindrical geometry of the vessels and compute n samples $S_{n,\mathbf{X},\mathbf{r},\mathbf{s}}$ around a point $\mathbf{X}$ with radius R by

$$S_{n,\mathbf{X},\mathbf{r},\mathbf{s}} = \{\mathbf{X} + R \cdot (\cos(i \cdot \frac{2\pi}{n}) \cdot \mathbf{r} + \sin(i \cdot \frac{2\pi}{n}) \cdot \mathbf{s})\} \quad (1)$$

for $i \in \{0, \ldots, n-1\}$, where $\mathbf{r}$ and $\mathbf{s}$ are the orthogonal generating vectors of the sampling plane. For sampling around a centerline point $\mathbf{C}$ of a vessel, we distinguish two possibilities to determine the local sampling plane given by the vectors $\mathbf{r}$ and $\mathbf{s}$. First, they can be chosen to be axis-aligned, for example, coinciding with the axial slice plane, i.e., $\mathbf{r} = (1,0,0)$ and $\mathbf{s} = (0,1,0)$. This leads to homogeneous surrounding regions outside the vessel lumen. If the vessel orientation is not perpendicular to the axis-aligned plane,

Figure 3: *Illustration of the sampling and aggregation around the centerline of a vessel. (a) displays a centerline with three cross-sectional planes. (b) demonstrates two sampling strategies, either with constant angle ω or with constant arc-length δ. (c) shows the circular ray profiles of the second cross-section with their maxima as squares and minima as dots. (d) presents the final image, where every cross-section is a row and every concentric circle a column. The maxima are displayed on the left side of the centerline and the minima on the right side.*

another sampling plane must be chosen, otherwise the surrounding information and the vessel lumen will be severely distorted. For this reason, and as the second possibility, we compute the rotation minimizing coordinate frame along the centerline using the double reflection method described by Wang et al. [WJZL08]. The circular rays are now orthogonal to the centerline, as shown in Figure 3a. Thus, the lumen of vessels with arbitrary orientation will not be distorted.

The concentric circular rays can be sampled at either constant angle or constant arc-length, as mentioned by Kanitsar et al. [KWFG03] and shown in Figure 3b. In the case of a constant angle ω, the sampling frequency remains fixed with increasing R, $n = (2\pi)/\omega$, but the distance between consecutive samples increases. When using constant arc-length sampling, $n = R \cdot U$, where U is the number of samples for $R = 1$. The sampling frequency increases with R, but the distance δ between two samples stays constant.
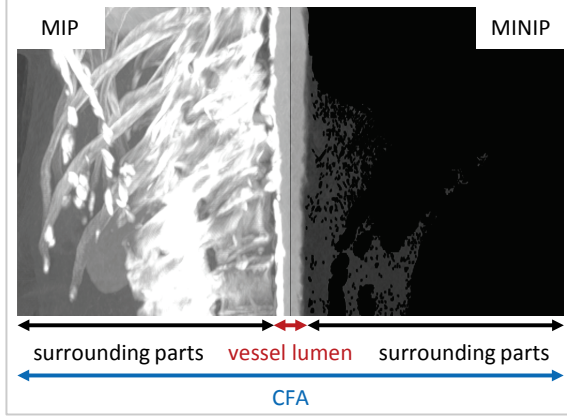
3.2. Aggregation

Radiologists usually browse through sets of many CPR images or axial slices. This inspection can be cumbersome and time-consuming due to the high number of images. Our new technique remedies this drawback. It aggregates features around the centerline and represents them in a single static image. This makes the rotation operation unnecessary. Since the centerline is defined by a curve, the technique is called Curvicircular Feature Aggregation (CFA). After specifying the samples for the circular rays, a single value needs
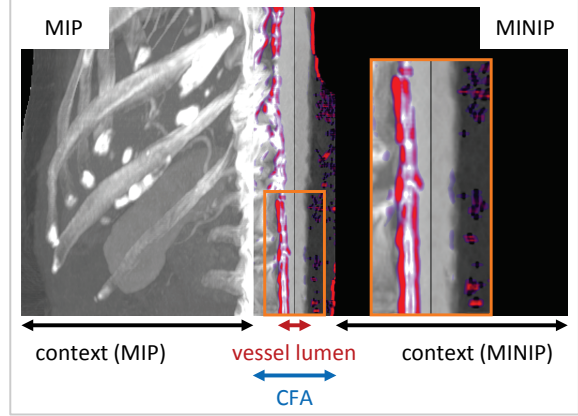
to be obtained for every ray by an aggregation operation. The goal is to extract relevant domain-specific information along such rays and convey it in the final image. Features of interest are mainly calcifications or soft plaque. Calcifications are well-characterized by the maximum intensity (MIP) along the ray, while soft plaque can be depicted by showing the minimum intensity (MINIP). While the average value could also provide additional information, the domain experts considered it less relevant in our experiments.

Figure 3 provides an overview of how the samples are aggregated and how the obtained values are placed in the resulting image. Figure 3a presents cross-sections along a vessel together with concentric circular rays and Figure 3b illustrates the two sampling strategies. Figure 3c shows the minima (dots) and maxima (squares) of the colored circular rays of cross-section 2. Figure 3d shows the placement of these values in the final image. The image can be divided into two parts, left and right, separated by the centerline. On the left side MIP is used and on the right MINIP. Both methods are *order independent*, i.e., regardless the direction of aggregating along a circular ray, the result stays the same. Due to this fact, two methods can be incorporated into a single image side-by-side. In the case of an *order dependent* technique, the results of the different directions would be shown on the left and right side of the image respectively. Since the rotation operation is not required, an orthogonal projection is used and the vessels are represented in a straightened way.

The aggregation is defined as an operator $Op(S_{n,\mathbf{X},\mathbf{r},\mathbf{s}}) = Op(D(v))$ over the intensities $D(v)$ for the samples $v \in$

Figure 4: *Example of CFA along a human abdominal aorta. The thin black centerline separates the image into two parts. MIP (left) shows how close calcifications approach the centerline and MINIP (right) displays the soft plaque.*

Figure 5: *Example of a context visualization outside the CFA and a stability overlay (from red to blue). The context rendering uses the same method as for the CFA.*

$S_{n,\mathbf{X},\mathbf{r},\mathbf{s}}$ of a circular ray. Figure 4 gives an example of MIP ($Op = max$) on the left and MINIP ($Op = min$) on the right side of the centerline. The left side highlights calcifications, whereas the right side shows soft plaque. Both features are clinically relevant and interesting. If there are high intensity values close to the centerline in MIP, the centerline passes through a calcification. This cannot happen if the centerline is properly specified to go through the blood flow channel, unless the vessel is completely blocked by an occlusion. The same holds for low intensity values close to the centerline, depicted this time with MINIP. Another possibility of aggregating along a ray is Average Intensity Projection (AVG), where $Op = mean$. However, calcifications and soft plaque are not so distinctly visible as compared to using MIP or MINIP. Additionally, no original data value is shown, which is not readily accepted in the medical domain.

3.3. Context

Since our method aggregates samples into a single value in a circular manner, spatial perception reduces with increasing distance from the vessel center. Motivated by the Vessel-Glyph [SKC*04] technique, which embeds a CPR (focus) into a MIP or DVR (context), we optionally augment the CFA (focus) of the vessel lumen with a context visualization of the vessels' surroundings. This contextual information enhances spatial perception and, for example, provides surgeons with a better overview of the vasculature. Figure 5 shows an example of a CFA with context visualizations on both sides. The final image $I_F(x,y)$ is composed by

$$I_F(x,y) = \begin{cases} I_{CFA}(x,y) & \text{if } |x_{cl} - x| \leq R_{max} \cdot f \\ I_{CTX}(x,y) & \text{if } |x_{cl} - x| > R_{max} \cdot f \end{cases} \quad (2)$$
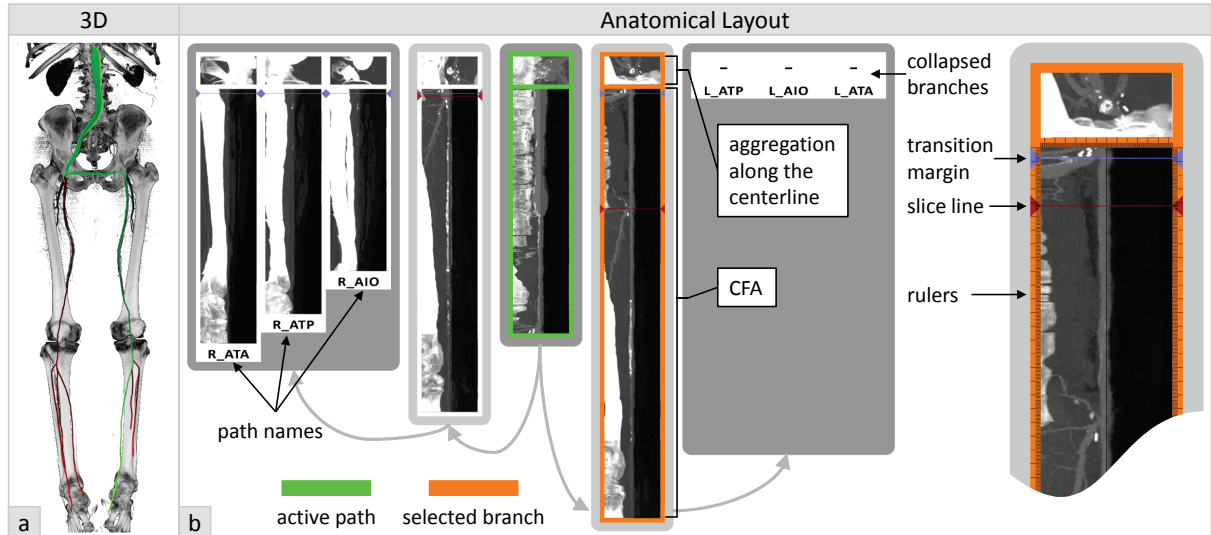
where I_{CFA} is the CFA image and I_{CTX} is the image of the context visualization, both with dimensions $W \times H$. The horizontal position of the centerline is $x_{cl} = W/2$. Because the vessel radius information is not always reliable, we multiply the maximum radius, R_{max}, of the current vessel branch by a user-specified factor f (2 in our implementation). This ensures that the context starts outside the vessel lumen. The context visualization is created by using axis-aligned raycasting (usually a frontal view of the data set).

3.4. Stability Analysis

A CFA crucially depends on the location of the centerline. Centerlines are typically available only with a certain accuracy. The stability of a CFA is determined by the magnitude of change that a slight variation of the centerline incurs on the resulting image. Since the centerline may not always be fully centered, we determine the CFA stability over a neighborhood of a centerline point $\mathbf{C}$. The neighbors $\mathbf{N}_{\mathbf{C},w}$ of $\mathbf{C}$ are computed as

$$\mathbf{N}_{\mathbf{C},w} = \{\mathbf{C} + i \cdot \mathbf{r}\} \times \{\mathbf{C} + j \cdot \mathbf{s}\} \quad (3)$$

for $i,j \in \{-w,\ldots,w\}$, where $w \in \mathbb{N}$ is user-specified and $\mathbf{r}$ and $\mathbf{s}$ are the orthogonal vectors generating the plane normal to the centerline. For each element of $\mathbf{N}_{\mathbf{C},w}$ we apply planar radial sampling and an operator Op to finally obtain an intensity value. The local stability is now given by the variance of all these values and describes the local uniformity around $\mathbf{C}$. The stability is low if the variance is high and vice versa. We overlay the CFA with the variance mapped to red if it is high and blue if it is low, as shown in Figure 5. A high variance close to the centerline indicates a badly estimated centerline. This can be used as an indicator for the centeredness of a centerline point.

Figure 6: *Anatomical layout of the human lower extremity vasculature with a cross-over bypass. (a) shows a 3D visualization together with the vessel tree. (b) presents the anatomical layout with the abdominal aorta (image with green border) in the middle and its branches placed to the left and right. The rightmost zoom-in uses a sampling plane orthogonal to the centerline to properly create the CFA of the bypass. It shows the transition margin, the slice line and the rulers inside the image borders.*

4. Visual Mapping

Finally, the whole tree-like vasculature of the human lower extremities should be presented in a meaningful and comprehensible way. Borkin et al. [BGP*11] propose a method where the branches of the vessel tree are connected at the axial slice positions of their parent branches. In our case, due to vessel straightening, this layout can become rather long. For this reason, the CFAs of the vasculature are spatially sorted from left to right (see Figure 6) and grouped according to anatomy. The root of the tree is centered and subsequent branches are presented to the left or right as a group. Because we render the vessel lumen straightened using orthogonal projection, distances can be measured easily and rulers are added to every CFA visualization. To allow the investigation of vessel branchings, every branch is prepended with a part of its parent vessel (10 points in our implementation). This is visually conveyed and delineated by the transition margin, as indicated by the blue line in Figure 6, leading to a 7mm overlap.

In addition to common interaction possibilities such as zooming, panning or changing the windowing function, whole branches of the vessel tree can be collapsed. The current user-selected vessel branch is highlighted in orange, whereas the path including it is marked as active and shown in green (see Figure 6). This path extends from the root to a leaf of the vessel tree. The context visualization and the centerline stability overlay can be interactively turned on and off by the user. While zooming is usually done by scaling the CFA texture and using texture interpolation capabilities,

we decrease the distances between consecutive circular rays starting from the centerline. This offers a denser sampling close to the centerline and provides a more precise zooming than texture interpolation. This changes only the horizontal scale and preserves the overview of the whole vessel branch.
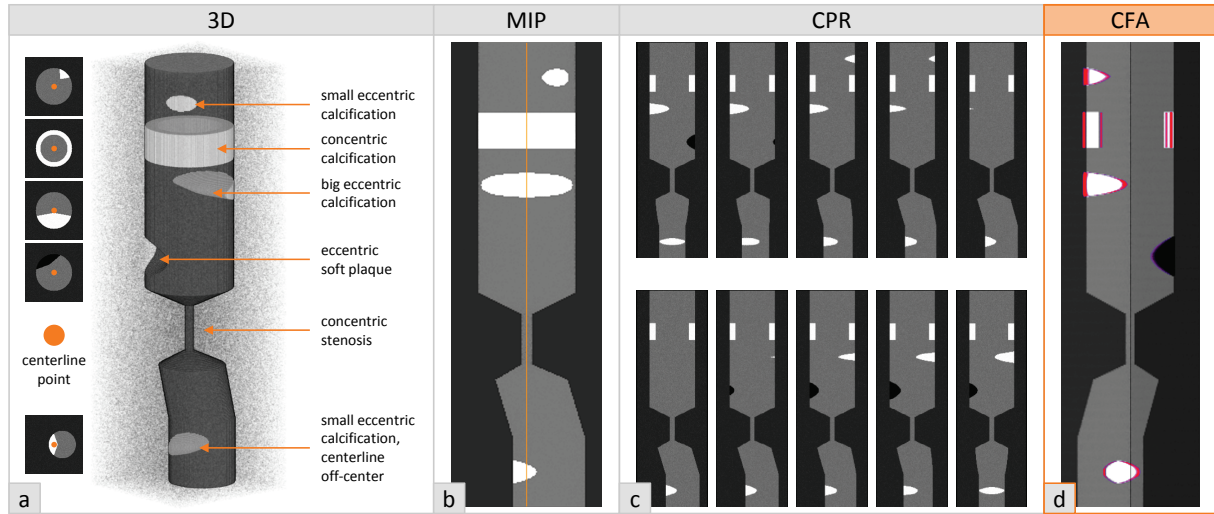
5. Results

We present results of CFA using three examples. First, we illustrate and demonstrate our method on a phantom data set containing several important pathological features. The second example shows the vasculature of the human pelvis including a vessel stenosis. Third, a vessel occlusion is presented below the bifurcation of the human abdominal aorta. In all examples MIP, CPR and CFA are compared.

5.1. Phantom Data Set

A phantom data set is shown in Figure 7. The centerline runs straight from top to bottom through the tube. The bottom of the tube is shifted sideways to simulate a centerline off-center. This can be seen by the orange centerline point inside the calcification at the bottom in Figure 7a. The following relevant pathological features are simulated (see Figure 7a):

- a small eccentric calcification,
- a concentric calcification,
- a big eccentric calcification,
- an eccentric soft plaque,
- a concentric stenosis and
- a small eccentric calcification, centerline off-center.

Figure 7: *A tubular phantom data set. (a) shows a 3D visualization of all relevant pathological features. (b) presents a MIP of the whole data set with the centerline in orange. (c) displays the CPR images and (d) the CFA with MIP on the left and MINIP on the right showing all the features within one image. A high variance (red) close to the centerline indicates that it is not properly centered.*

In the MIP in Figure 7b the concentric calcification seems to block the whole vessel. Even the big eccentric calcification appears to prevent any blood flow. This can be clarified by using CPR or CFA. The CPR images in Figure 7c are generated for angles from $-90°$ to $90°$ with an $18°$ stepsize. It is cumbersome inspecting all these images and judging, for example, the centeredness of the centerline.

CFA is shown in Figure 7d with MIP on the left side and MINIP on the right side. The sampling planes of the circular rays correspond to the axial slices. All calcifications can be seen on the left and the soft plaque on the right. If a calcification is visible in MIP and MINIP close to the vessel wall, then it is a concentric calcification. If a calcification is only visible in MIP, it is an eccentric one. The same can be observed for soft plaque, but with MINIP. Additionally, it is possible to judge the centeredness of the centerline. Because the eccentric calcification at the bottom also appears in the MINIP, but close to the centerline rather than close to the vessel wall, the centerline has to pass through the calcification, although it should not. The centerline is not properly centered in this part, because it should always be in the vessel lumen. The high variance (red) at the centerline supports this conclusion.

5.2. Vessel Stenosis

Figure 8 shows a CTA data set of the human pelvis with a vessel stenosis. The position of the stenosis is pointed out by an arrow in the top-left 3D visualization. Next, axial slices at the beginning, at the center, and at the end of the stenosis are presented. They show how the lumen narrows in the center
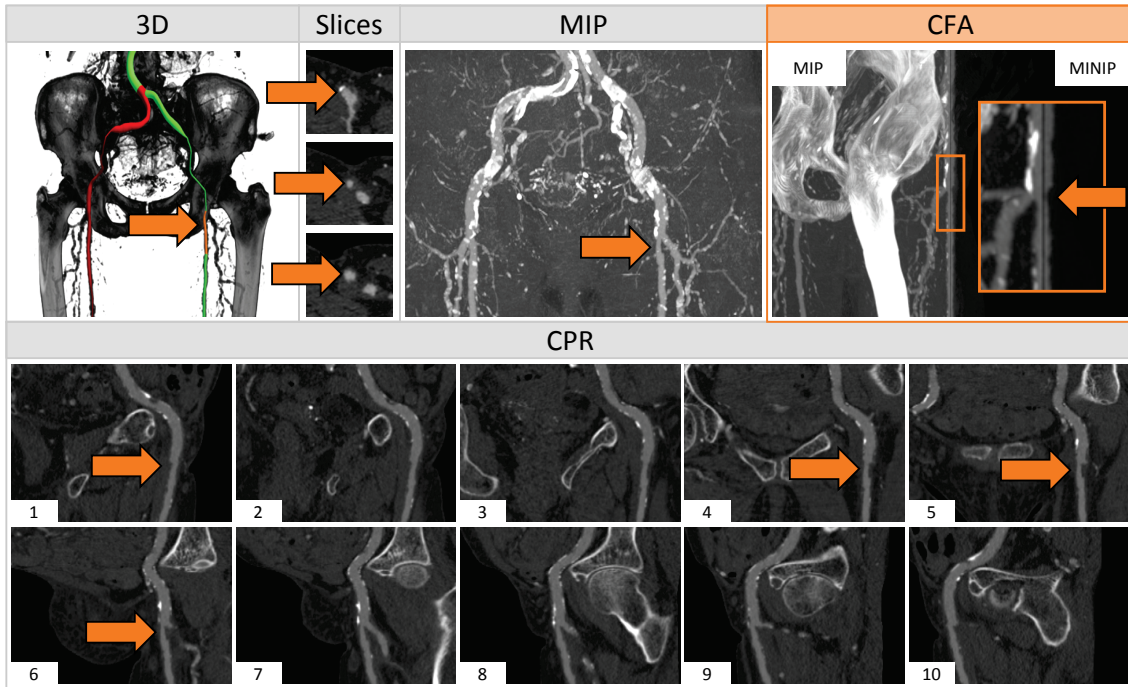
of the stenosis. In the MIP image the stenosis is hardly perceivable. The CFA image at the top-right shows a MIP on the left side and a MINIP on the right side. Again, an axial slice aligned sampling plane is used. It is well perceivable in the zoom-in, where and how much the vessel becomes narrow (orange arrow). The CPR images at the bottom of Figure 8 are generated for the angles between $-90°$ and $90°$ with a stepsize of $18°$.

5.3. Vessel Occlusion
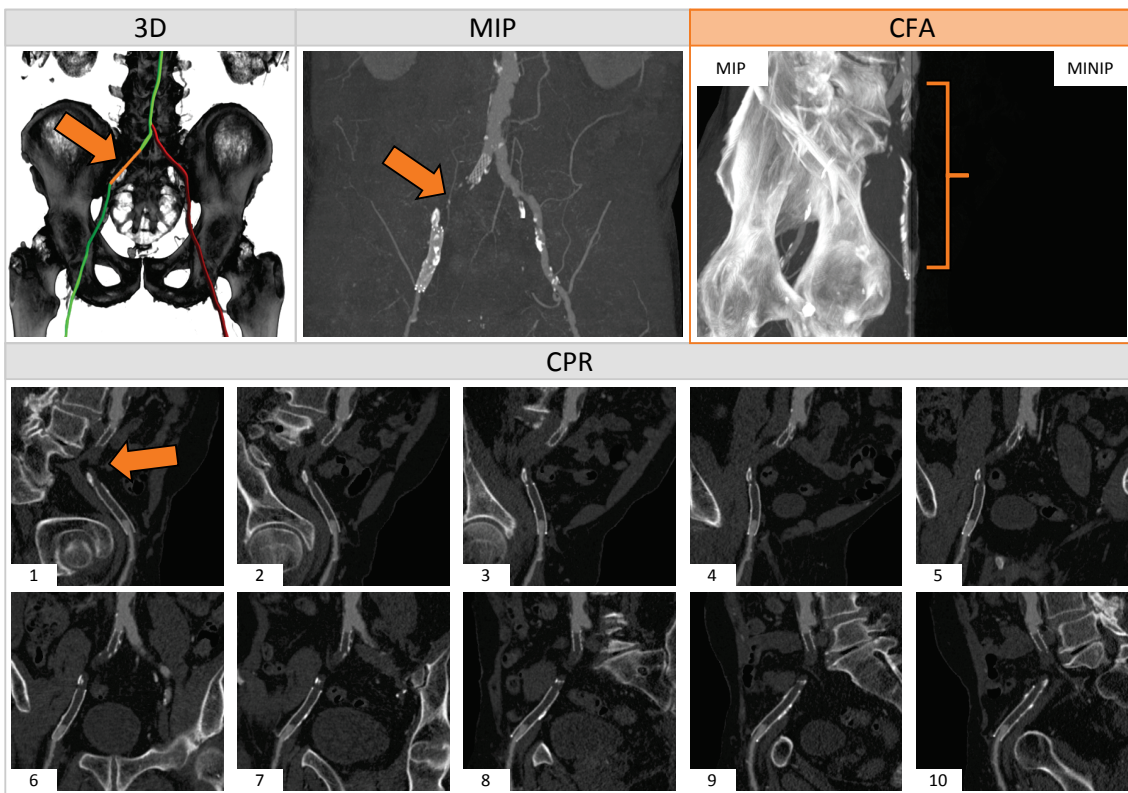
Figure 9 presents a CTA data set of the human pelvis with a vessel occlusion inside a stent below the bifurcation of the abdominal aorta. The occlusion is highlighted by an arrow in the top-left 3D visualization and even clearly visible in the MIP image, but the lumen inside the stent remains obscured. The CPR images (between $-90°$ and $90°$ with an $18°$ stepsize) show the occlusion well, but many of them have to be inspected. In contrast, the CFA shows the entire occlusion within one image. Since soft plaque is visible on both sides up to the vessel wall and its intensity differs from blood, it can only be a concentric stenosis inside the stent obstructing the whole lumen and preventing blood from flowing.

6. Discussion and Limitations
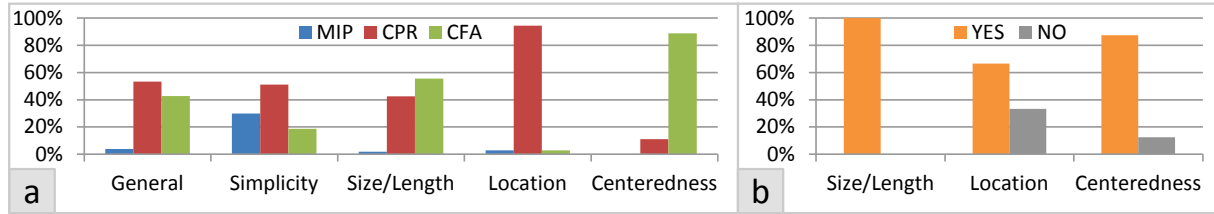
One drawback of CFA originates from the aggregation along the circular rays. If using an order independent aggregation, the exact circular location of a feature is not conveyed in the final image. MIP, for example, captures only the maximum value along the ray, regardless of its position and size. To

Figure 8: *A CTA data set of the human pelvis with a vessel stenosis pointed out by the orange arrows.*

Figure 9: *A human pelvic CTA data set with a vessel occlusion pointed out by the orange arrows and the bracket.*

Figure 10: *Evaluation of CFA. (a) shows the overall evaluation concerning five categories. (b) presents the clinical relevance of three categories. The y-axes show the ratings in percent (%) given by the participants.*

determine the exact location within a cross-section, we provide clinicians with additional linked views, for example, an axial slice view.

Furthermore, CFA is much less sensitive to changes of the centerline than CPR and additionally provides information about the centerline stability by visually guiding users to highly varying regions. Large errors in the centerline detection cause problems, for example, if the centerline is outside the vessel lumen. However, with CPR the pathological feature at the bottom of the phantom data set (Figure 7c) might be reported as a stenosis, although it is a pseudo stenosis. In fact, this case is one of the motivations for our technique, because through using MIP and MINIP it is possible to judge the centeredness of the centerline. Hence, the centerline stability is less of an issue for CFA.

7. Evaluation

We consulted nine radiologists for an evaluation of CFA with a questionnaire. We compared MIP with CPR and CFA concerning the pathological features presented in the phantom data set (Figure 7) and concerning the vessel stenosis (Figure 8) and the vessel occlusion (Figure 9). Additional linked slice views were not used in this comparison. The questionnaire consisted of 48 questions summarized in five categories (see Figure 10a). The usefulness of three of these categories has been evaluated separately (see Figure 10b).

In the assessment of overall preference (labeled *General*), CPR performs better than CFA and both are significantly better than MIP. The reason for this could be that CFA has been mostly new to the participants and MIP and CPR have already been well known. The evidence for this is given by the next category: simplicity. CPR is seen as the most simple method, followed by MIP and finally CFA. More learning time is probably required to understand CFA and then interpret the images accordingly. Two radiologists specifically mentioned that, after the initial accommodation period, the technique shows great potential.

The strengths of CFA are the possibility to immediately measure the size or length of a stenosis and the analysis of the centeredness of a centerline. Both are well indicated in the evaluation. As mentioned in the limitations of CFA, the

location of a pathology within a cross-section cannot be estimated properly without linked slice views. CPR performed best by far in this category.

Figure 10b shows the results of the feedback regarding the usefulness of the following three categories. All participants rated the size and length of a stenosis as useful, whereas only some did this for the cross-sectional location. Two radiologists confirmed that the position along the centerline is more important than the one within the cross-section. The cross-sectional location is not considered to be relevant for current therapeutic procedures in the clinical routine (balloon dilatation, stenting, and bypass surgery). Most participants see the analysis of the centeredness of a centerline as useful. The strengths of CFA are seen as very useful and received a positive response. The feedback obtained from domain experts gives an indication that CFA could be a valuable alternative to MIP and CPR in the clinical routine.

8. Conclusion

In this paper we introduced Curvicircular Feature Aggregation (CFA), a new technique for the visualization of blood vessels. Our novel approach aggregates vessel features around the centerline into a single static image. This avoids inspecting the vessel lumen from multiple viewing angles. Furthermore, our method provides additional visual cues on the centerline stability. We describe how such an aggregation of a vessel tree can be presented anatomically sorted and grouped and suggest linked views for further visual analysis. Domain expert feedback indicates that our method can be an alternative to MIP and CPR.

References

[BFC04] BÜHLER K., FELKEL P., CRUZ A. L.: *Geometric Methods for Vessel Visualization and Quantification - A Survey*. Springer, 2004, ch. in Geometric Modeling for Scientific Visualization, pp. 399–419. 2

[BGP*11] BORKIN M. A., GAJOS K. Z., PETERS A., MITSOURAS D., MELCHIONNA S., RYBICKI F. J., FELDMAN C. L., PFISTER H.: Evaluation of artery visualizations for heart disease diagnosis. *IEEE Trans. Vis. Comput. Graphics 17*, 12 (2011), 2479–2488. 2, 6

[BS91] BLOOMENTHAL J., SHOEMAKE K.: Convolution surfaces. *SIGGRAPH Comput. Graph. 25*, 4 (1991), 251–256. 2

[BWKG01] BARTROLÍ A. V., WEGENKITTL R., KÖNIG A., GRÖLLER E.: Nonlinear virtual colon unfolding. In *Proceedings of IEEE Visualization* (2001), pp. 411–420. 2

[DKT98] DEROSE T., KASS M., TRUONG T.: Subdivision surfaces in character animation. In *Proceedings of the 25th annual conference on Computer graphics and interactive techniques* (1998), ACM, pp. 85–94. 2

[FWB04] FELKEL P., WEGENKITTL R., BÜHLER K.: Surface models of tube trees. In *Proceedings of Computer Graphics International* (2004), pp. 70–77. 2

[Grö95] GRÖLLER M. E.: Nonlinear raytracing - visualizing strange worlds. *Visual Computer 11*, 5 (1995), 263–274. 2

[HGQ*06] HONG W., GU X., QIU F., JIN M., KAUFMAN A.: Conformal virtual colon flattening. In *Proceedings of the 2006 ACM symposium on Solid and physical modeling* (2006), SPM '06, ACM, pp. 85–93. 2

[HMC11] HSU W.-H., MA K.-L., CORREA C.: A rendering framework for multiscale views of 3d models. *ACM Trans. Graph. 30*, 6 (2011), 131:1–131:10. 2

[HPP*00] HÖHNE K. H., PFLESSER B., POMMERT A., RIEMER M., SCHUBERT R., SCHIEMANN T., TIEDEAND U., SCHUMACHER U.: A realistic model of the inner organs from the visible human data. In *Proceedings of the Third International Conference on Medical Image Computing and Computer-Assisted Intervention* (2000), MICCAI '00, Springer-Verlag, pp. 776–785. 2

[HPSP01] HAHN H. K., PREIM B., SELLE D., PEITGEN H.-O.: Visualization and interaction techniques for the exploration of vascular structures. In *IEEE Visualization 2001* (2001), pp. 395–402. 2

[KBF*08] KLEIN J., BARTZ D., FRIMAN O., HADWIGER M., PREIM B., RITTER F., VILANOVA A., ZACHMANN G.: Advanced algorithms in medical computer graphics. In *Proceedings of Eurographics* (2008), pp. 25–44. 2

[KFW*01] KANITSAR A., FLEISCHMANN D., WEGENKITTL R., SANDNER D., FELKEL P., GRÖLLER E.: Computed tomography angiography: a case study of peripheral vessel investigation. In *Proceedings of IEEE Visualization* (2001), pp. 477–593. 3

[KFW*02] KANITSAR A., FLEISCHMANN D., WEGENKITTL R., FELKEL P., GRÖLLER M. E.: CPR - curved planar reformation. In *Proceedings of IEEE Visualization* (2002), pp. 37–44. 1, 2, 3

[KFWG06] KANITSAR A., FLEISCHMANN D., WEGENKITTL R., GRÖLLER M. E.: Diagnostic relevant visualization of vascular structures. In *Scientific Visualization: The Visual Extraction of Knowledge from Data*, Bonneau G.-P., Ertl T., Nielson G., (Eds.), Mathematics and Visualization. Springer Berlin Heidelberg, 2006, pp. 207–228. 1, 2

[KPL94] KIM M.-S., PARK E.-J., LEE H.-Y.: Modeling and animation of generalized cylinders with variable radius offset space curves. *Journal of Visualization and Computer Animation 5*, 4 (1994), 189–207. 2

[KWFG03] KANITSAR A., WEGENKITTL R., FLEISCHMANN D., GRÖLLER E.: Advanced curved planar reformation: Flattening of vascular structures. In *Proceedings of IEEE Visualization* (2003), pp. 43–50. 2, 4

[KY95] KURZION Y., YAGEL R.: Space deformation using ray deflectors. In *6th Eurographics Workshop on Rendering 95* (1995), Springer, pp. 21–32. 2

[LC87] LORENSEN W. E., CLINE H. E.: Marching cubes: A high resolution 3d surface construction algorithm. *SIGGRAPH Comput. Graph. 21*, 4 (1987), 163–169. 2

[LCMH09] LAMPE O. D., CORREA C., MA K.-L., HAUSER H.: Curve-centric volume reformation for comparative visualization. *IEEE Transactions on Visualization and Computer Graphics 15*, 6 (2009), 1235–1242. 2

[LG96] LÖFFELMANN H., GRÖLLER E.: Ray tracing with extended cameras. *The Journal of Visualization and Computer Animation 7*, 4 (1996), 211–227. 2

[PO07] PREIM B., OELTZE S.: *3D Visualization of Vasculature: An Overview*. Springer, 2007, ch. Visualization in Medicine and Life Science, pp. 19–39. 2

[PSH*04] PORTUGALLER H. R., SCHOELLNAST H., HAUSEGGER K. A., TIESENHAUSEN K., AMANN W., BERGHOLD A.: Multislice spiral CT angiography in peripheral arterial occlusive disease: a valuable tool in detecting significant arterial lumen narrowing? *European Radiology 14*, 9 (2004), 1681–1687. 3

[RFK*07] ROOS J. E., FLEISCHMANN D., KÖCHL A., RAKSHE T., STRAKA M., NAPOLI A., KANITSAR A., SRAMEK M., GRÖLLER E.: Multi-path curved planar reformation (mpCPR) of the peripheral arterial tree in CT angiography (CTA). *Radiology 244*, 1 (2007), 281–290. 2

[SKC*04] STRAKA M., KÖCHL A., CERVENANSKY M., SRAMEK M., FLEISCHMANN D., CRUZ A. L., GRÖLLER E.: The VesselGlyph: Focus & Context Visualization in CT-Angiography. In *Proceedings of IEEE Visualization* (2004), pp. 385–392. 5

[TOBB*07] TERMEER M., OLIVÁN BESCÓS J., BREEUWER M., VILANOVA A., GERRITSEN F., GRÖLLER E.: CoViCAD: Comprehensive visualization of coronary artery disease. *IEEE Trans. Vis. Comput. Graphics 13*, 6 (2007), 1632–1639. 2

[WGC*08] WILLIAMS D., GRIMM S., COTO E., ROUDSARI A., HATZAKIS H.: Volumetric curved planar reformation for virtual endoscopy. *IEEE Trans. Vis. Comput. Graphics 14*, 1 (2008), 109–119. 2

[WJZL08] WANG W., JÜTTLER B., ZHENG D., LIU Y.: Computation of rotation minimizing frames. *ACM Trans. Graph. 27*, 1 (2008), 2:1–2:18. 4

[WMM*10] WUA J., MAA R., MAA X., JIA F., HUA Q.: Curvature-dependent surface visualization of vascular structures. *Computerized Medical Imaging and Graphics 34* (2010), 651–658. 2

[WSE04] WEISKOPF D., SCHAFHITZEL T., ERTL T.: GPU-based nonlinear ray tracing. *Comput. Graph. Forum 23*, 3 (2004), 625–634. 2

[WZMK05] WANG L., ZHAO Y., MUELLER K., KAUFMAN A.: The magic volume lens: An interactive focus+context technique for volume rendering. In *Proceedings of IEEE Visualization* (2005), pp. 367–374. 2